Research article

NMR IN BIOMEDICINE

Received: 05 June 2013, Revised: 11 November 2013, Accepted: 12 November 2013, Published online in Wiley Online Library: 8 December 2013

(wileyonlinelibrary.com) DOI: 10.1002/nbm.3060

MRI of neonatal necrotizing enterocolitis in a rodent model

Devkumar Mustafi[a], Sheng-Ru Shiou[b], Xiaobing Fan[a], Erica Markiewicz[a], Gregory S. Karczmar[a] and Erika C. Claud[b,c]*

Neonatal necrotizing enterocolitis (NEC) is a poorly understood life-threatening illness afflicting premature infants. Research is hampered by the absence of a suitable method to monitor disease progression noninvasively. The primary goal of this research was to test *in vivo* MRI methods for the noninvasive early detection and staging of inflammation in the ileum of an infant rat model of NEC. Neonatal rats were delivered by cesarean section at embryonic stage of day 20 after the beginning of pregnancy and stressed with formula feeding, hypoxia and bacterial colonization to induce NEC. Naturally born and dam-fed neonatal rats were used as healthy controls. *In vivo* MRI studies were performed using a Bruker 9.4-T scanner to obtain high-resolution anatomical MR images using both gradient echo and spin echo sequences, pixel-by-pixel T_2 maps using a multi-slice–multi-echo sequence, and maps of the apparent diffusion coefficient (ADC) of water using a spin echo sequence, to assess the degree of ileal damage. Pups were sacrificed at the end of the MRI experiment on day 2 or 4 for histology. T_2 measured by MRI was increased significantly in the ileal regions of pups with NEC by histology (106.3 ± 6.1 ms) compared with experimentally stressed pups without NEC (85.2 ± 6.8 ms) and nonstressed, control rat pups (64.9 ± 2.3 ms). ADC values measured by diffusion-weighted MRI were also increased in the ileal regions of pups with NEC by histology [(1.98 ± 0.15) × 10^{-3} mm^2/s] compared with experimentally stressed pups without NEC [(1.43 ± 0.16) × 10^{-3} mm^2/s] and nonstressed control pups [(1.10 ± 0.06) × 10^{-3} mm^2/s]. Both T_2 and ADC values between these groups were found to be significantly different ($p < 0.03$). The correlation of MRI results with histologic images of the excised ileal tissue samples strongly suggests that MRI can noninvasively identify NEC and assess intestinal injury prior to clinical symptoms in a physiologic rat pup model of NEC. © 2013 The Authors. *NMR in Biomedicine* published by John Wiley & Sons, Ltd.

Keywords: apparent diffusion coefficient; diffusion-weighted imaging; MRI; necrotizing enterocolitis; neonatal rat pups

INTRODUCTION

Necrotizing enterocolitis (NEC) is a life-threatening inflammatory bowel disorder of unknown cause that affects approximately 10% of premature infants (weight at birth < 1500 g) and carries a mortality rate of 20–30% (1–4). The pathophysiology of this disease is poorly understood. The most widely accepted animal model is a physiologic rat model of NEC which recapitulates many of the stresses placed on preterm infants (5–11). To simulate the clinical risk factors for NEC, rat pups are formula fed, colonized with bacteria and asphyxia stressed three times a day. With this model, about 30% of the pups develop NEC as determined by a well-defined histologic scoring system of intestinal tissue (11). However, as this model requires sacrifice of the pups for the diagnosis of NEC, the ability to monitor disease progression or to test treatment interventions is precluded. A noninvasive tool to diagnose intestinal injury prior to clinical symptoms is critical to obtain an improved understanding of the mechanism of NEC and therapeutic interventions.

Noninvasive MRI methods can be used to reliably detect intestinal injury with high contrast (12). MRI has several advantages over other cross-sectional imaging techniques, particularly computed tomography (13,14). Compared with computed tomography, MRI provides higher contrast-to-noise ratio and excellent soft tissue contrast combined with high spatial resolution (15,16). More importantly, the absence of ionizing radiation makes MRI an attractive method (17–19). To our knowledge, there has been no published MRI study of NEC in any animal model; only one MRI study of preterm infants with NEC has been reported in the literature (20), in which a 'bubble-like' appearance in MR images at the site of intestinal necrosis at surgery was observed (20). This previous study did not explore the use of MRI to demonstrate intestinal injury prior to the onset of clinical symptoms or the need for surgical intervention.

* *Correspondence to: E. C. Claud, Department of Pediatrics and Medicine, University of Chicago, 5841 S. Maryland Avenue, MC6060, Chicago, IL 60637, USA. E-mail: eclaud@peds.bsd.uchicago.edu*

a *D. Mustafi, X. Fan, E. Markiewicz, G. S. Karczmar*
Department of Radiology, University of Chicago, Chicago, IL, USA

b *S.-R. Shiou, E. C. Claud*
Department of Pediatrics, University of Chicago, Chicago, IL, USA

c *E. C. Claud*
Department of Medicine, University of Chicago, Chicago, IL, USA

Abbreviations used: *ADC, apparent diffusion coefficient; DWI, diffusion-weighted imaging; FSE, fast spin echo; GE, gradient echo; MSME, multi-slice–multi-echo; NEC, necrotizing enterocolitis; ROI, region of interest; T_2, spin–spin relaxation time.*

The primary objective of this work was to test *in vivo* MRI methods as a tool for the early detection and staging of inflammation in the ileum of an infant rat model of NEC. The study of the rat pup model reported here will facilitate future studies to improve our understanding of NEC – specifically the progression of disease and response to therapy – and lay the groundwork for the exploration of MRI as a predictive diagnostic tool for the imaging of preterm infants at risk for NEC. In our previous MRI studies, we demonstrated that the morphologic data from T_2-weighted MR images, together with contrast-enhanced MRI data, can differentiate inflamed bowel from normal bowel in a murine model of ulcerative colitis (12). Inflammation was identified on the basis of measurements of colon wall thickness, increases in T_2 caused by edema, together with a faster volume transfer rate and a larger volume of distribution of contrast medium, using a gadolinium-based contrast agent at 9.4 T (12). The use of contrast media is not feasible in the <5-day-old rat pup model, and the colon wall thickness in both control and NEC rat pups is too small (~40–50 μm) to measure accurately. Thus, in the present study, diffusion-weighted imaging (DWI) was used to complement the results obtained from T_2-weighted images and T_2 relaxation time maps. DWI is predicted to be sensitive to edema, because it measures the apparent diffusion coefficient (ADC) of water as a marker of changes in cell density caused by inflammation (21).

MATERIALS AND METHODS

Ethics statement

This study was carried out in strict accordance with the recommendations in the Guide for the Care and Use of Laboratory Animals of the National Institutes of Health. All animal work was approved by the University of Chicago Institutional Animal Care and Use Committee. Cesarean section was performed under isoflurane anesthesia, and all efforts were made to minimize suffering. If a rat pup showed illness during the course of the study, the animal was humanely euthanized.

Neonatal rat NEC model

Animal experiments were conducted following a well-described rat NEC animal model (5,6). In this model, pups were subjected to major risk factors for human NEC (prematurity, formula feeding, bacterial colonization and hypoxia–ischemia), resulting in intestinal injury in immature rat pups similar to that found in humans as follows: the abdomen was distended; blood was detected in the stool; and the ileum and proximal colon were the most affected parts of the intestine (22).

Neonatal rats from time-dated pregnant Sprague-Dawley dams were delivered by cesarean section at E20 (embryonic stage of day 20 after the beginning of pregnancy) following isoflurane anesthesia. Pups were then stabilized, dried and maintained in a humidified incubator at 37 °C, and bowel/bladder function was stimulated by a soft cotton-tip applicator. Pups were fed with Esbilac puppy formula every 3 h via an orogastric feeding catheter and colonized with 10^7 colony forming units of *Serratia marcescens*, *Klebsiella pneumoniae* and *Streptococci viridans* in 100 μL formula once daily. Pups were also stressed under 5% O_2 + 95% N_2 for 10 min after feeding three times a day. The feeding volume began at 0.1 mL and was increased incrementally up to 0.25 mL. Naturally born rat pups fed by dams were included as healthy controls (5,11).

Fifty-one rat pups (2–4 days old) were used in this study. Fifteen naturally born rat pups were used as healthy controls, and 36 rat pups which had been exposed to the stress of the NEC model were included. Of 36 rat pups that were prematurely born, formula fed and stressed, $n = 20$ pups had no sign of NEC on histology or intestinal inflammation by MRI; these pups were used as experimental controls (NEC score of 0); $n = 5$ pups were found without histologic NEC (histologic NEC score of 0), but ileal wall edema was detected by MRI in the ileum; these pups were used as a separate group and termed 'pre'-NEC; $n = 5$ pups were found with a histologic NEC score of 1, $n = 3$ pups with a histologic NEC score of 2 and $n = 3$ pups with a histologic NEC score of 3. As this is a physiologic model in which stresses relevant to preterm infants (formula feeding, bacterial colonization, hypoxia stress) are applied to the rodent pups, rather than a discrete point of injury, there is variable response.

Tissue harvesting and immunohistochemistry

As per protocol, animals were sacrificed after MRI scanning for the correlation of MRI results with histologic scoring. The intestines were collected and fixed in 10% buffered formalin overnight for tissue section preparation. Hematoxylin and eosin-stained intestinal sections were assessed histologically for ileal damage by a pathologist blinded to treatment group using a published NEC scoring system to evaluate the degree of intestinal injury on a '0–4' scale as follows: 0, no necrosis; 1, mild with epithelial sloughing; 2, moderate with mid-villous necrosis; 3, severe with total villous necrosis; 4, transmural necrosis. Scores ≥ 2 are defined as NEC. The NEC incidence of the animal model performed in our studies is consistent with previous published reports using this model (6). Histologic NEC scores were based on histopathology of the excised ileum immediately following *in vivo* MRI studies.

In vivo MRI

MRI studies were performed using a Bruker Biospec (Billerica, MA, USA) 33-cm horizontal-bore scanner with 12-cm bore, high-performance, self-shielded gradients (maximum gradient strength, 100 mT/m) at 9.4 T. A Bruker quad coil (35 mm) was used for *in vivo* imaging (12,23). Rat pups were anesthetized during procedures with 0.5–1% isoflurane mixed with medical air to maintain a surgical plane of anesthesia. No paralytic agents were used. Temperature was monitored continuously by a thermometer and controlled with warm air. The respiration rate was monitored with an optical detection system from SA Instruments (Stony Brook, NY, USA), developed for use in *in vivo* MRI.

High-resolution MR images of the ileum, adjacent to the cecum, of neonatal rat pups were acquired with multi-slice gradient echo (GE) and fast spin echo (FSE) sequences in coronal and axial orientations, respectively. To acquire coronal images, we found that a GE sequence provides anatomical references with no or little motion artifact, whereas FSE provides high spatial resolution axial images that can be used to measure the degree of inflammation. As, in some cases, the changes appear in small regions, we acquired images with slice thicknesses of 0.5 mm and 0.25 mm in scans 2 and 3, respectively, as listed in Table 1. In each case, we selected a small area of 0.5–0.6 mm^2 (with about 85–105 pixels) of the ileal section adjacent to the cecum as the region of interest (ROI) for the measurement of T_2 and ADC values. The experimental parameters for *in vivo* MRI measurements are given in Table 1. High-resolution anatomical MR

Table 1. A typical experimental protocol for the acquisition of MR images of 3-day-old rat pups[a]

Scan	Type	TR/TE (ms)	No. of slices	Field of view (mm^2)	Matrix size	Slice thickness (mm)	In-plane resolution (μm)	Number of averages
1	GE	500/5	11	25.6 × 12.8	256 × 128	1.0	100	1
2	FSE	4000/27	21	25.6 × 12.8	256 × 128	0.5	100	2
3	FSE	4000/27	41	20 × 10	256 × 128	0.25	78	4
4	MSME[b]	5000/10	9	25.6 × 12.8	128 × 64	0.5	200	2
5	DWI	4500/26	9	25.6 × 12.8	128 × 64	0.5	200	2

[a]This protocol takes about 1 h 15 min for data acquisition. GE, gradient echo with a spoiled FLASH (fast low-angle shot) sequence with a flip angle of 20° and with fat saturation; FSE, fast spin echo with refocused echoes with a four-echo train and with fat saturation; MSME, multi-slice–multi-echo without fat saturation; DWI, diffusion-weighted imaging using a spin echo sequence without fat saturation. The first scan was in the coronal plane; all other scans (2–5) were in the axial orientation.
[b]The spin echo methods provide accurate results for T_2 measurements reported here. However, the measured intensity ($M_{x,y}$) at the first TE is often underestimated. This would be a real concern for tissue samples with T_2 values in the range 20–25 ms, such as muscle. However, in our studies, we determined values of T_2 in the range 65–110 ms.

images guided the slice selection for T_2 measurements and DWI. Spin–spin relaxation times (T_2) were determined using a multi-slice–multi-echo (MSME) sequence (200 μm in-plane resolution with 0.5 mm slice thickness) with 32 TEs ranging between 10 and 400 ms. Values of T_2 were calculated from plots of the measured intensities ($I_{x,y}$) as a function of TE, according to Equation [1]:

$$I_{x,y} = I_0[\exp(-\mathrm{TE}/T_2)] \quad [1]$$

where I_0 is the signal intensity at TE = 0 ms.

Diffusion-weighted images were acquired using a spin echo sequence without fat suppression and with b values of 0, 250, 500 and 1000 s/mm^2, with the same spatial resolution as for T_2 measurements. DWI was used to measure the ADC of water. Values of ADC (D) were calculated from plots of the measured signal intensity (I) as a function of the b value, according to Equation [2]:

$$I = I_0[\exp(-D \cdot b)] \quad [2]$$

where I_0 is the intensity at b = 0 s/mm^2.

As listed in Table 1, the matrix size in the phase encoding direction was half of the matrix size in the readout direction in both MSME and DWI sequences. This decreased image acquisition time and reduced motion artifacts. In addition, images were acquired with two averages to significantly increase the signal-to-noise ratio and image quality. ADC is sensitive to changes in cell density and microarchitecture associated with edema and the reorganization of crypts (24).

Data and statistical analysis

Data analysis was performed with software written in IDL (Research Systems, Inc., Boulder, CO, USA). Two investigators drew ROIs manually and independently measured values for T_2 and ADC. In addition, as we used the spin echo sequence in both MSME and DWI, the same set of ROIs was selected for the measurement of T_2 and ADC values. The investigators were blinded to the NEC scores when they selected the ROIs. ROIs were selected on the basis of T_2 and ADC values only. Later, histopathologic assignments of NEC scores were performed. Average values with standard deviations were calculated, and two-way analysis of variance was performed between groups for statistical analysis. A confidence interval of $p < 0.05$ was considered to be statistically significant.

RESULTS

Histologic evaluation based on the degree of disruption of the epithelial villi demonstrated significant differences between

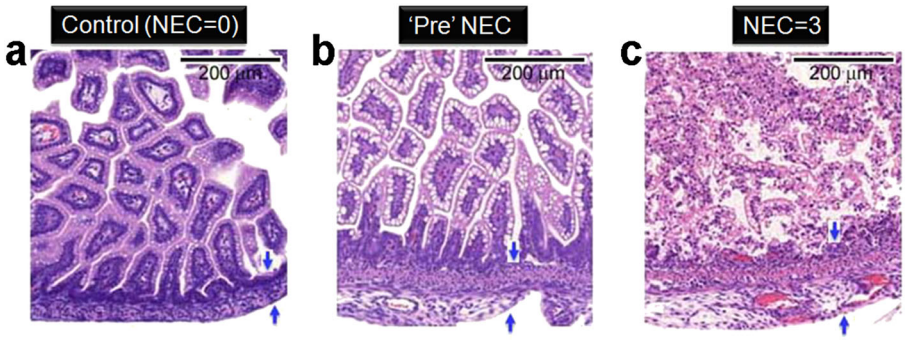

Figure 1. Rat model of necrotizing enterocolitis (NEC) demonstrates variability in histologic findings that could be correlated with MRI. Hematoxylin and eosin-stained images of ileal sections are illustrated for a control rat pup (NEC score of 0) (a), a nonsymptomatic rat pup exposed to the stresses of the NEC model, with early-stage intestinal alteration as demonstrated by expansion of the submucosal layer (indicated by blue arrows), but no villus disruption (termed 'pre'-NEC) (b), and a symptomatic rat pup with NEC, as noted by both the submucosal space expansion and villus disruption (NEC score of 3) (c). The term 'pre'-NEC is used when pups do not have any histologic sign of NEC, but MRI shows significant edema, as measured by T_2 and apparent diffusion coefficient (ADC) values.

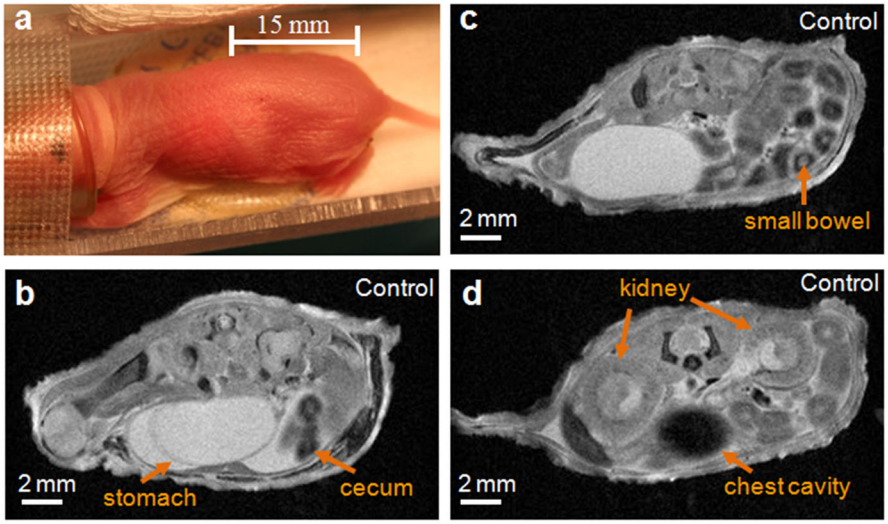

Figure 2. Photograph (a) of a control pup placed on a platform (temperature-resistant garolite holder) before insertion into the quad coil and the magnet, and MR images (b–d) of the same pup. MR images were acquired from near the rectum area to the end of the abdominal area/beginning of the chest cavity; the length of the imaged area was about 15 mm, as indicated by the ruler in (a). The stomach, cecum, small bowel, kidneys and chest cavity are labeled in (b)–(d). No inflammation was detected either in the ileum near the cecum or in the small bowel.

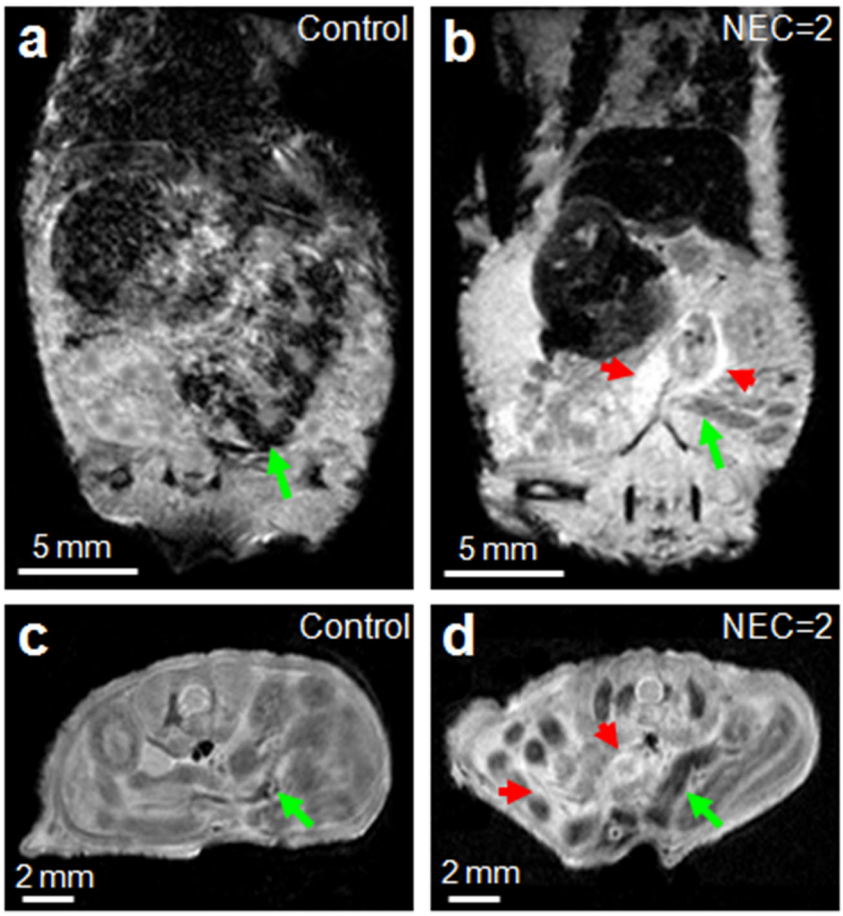

Figure 3. MR images of a naturally born, mother-fed, control rat pup and a premature, formula-fed, stressed, 3-day-old rat pup of the necrotizing enterocolitis (NEC) model. (a, b) Two MR images that were acquired with a gradient echo sequence in a coronal orientation for a mother-fed, control pup (NEC score of 0) and a NEC pup (score of 2), respectively. (c, d) Two MR images that were acquired with a spin echo sequence in an axial plane for the corresponding pups as in (a, b). All MRI parameters are given in Table 1. In both panels, brighter, inflamed regions of the ileum, adjacent to the cecum, are indicated by red arrows, whereas green arrows indicate the cecum. Following *in vivo* MRI studies, the rat pup with NEC was sacrificed and the ileum was excised for hematoxylin and eosin staining. The pathologic NEC score of 2 for this pup, as in the MR images in (b) and (d), was assigned independently by a pathologist at the University of Chicago Medical Center.

control and treated pups. Figure 1 compares histologic images of a healthy control pup (Fig. 1a), a stressed nonsymptomatic rat pup with no detectable NEC by traditional histologic scoring (see Materials and methods section) (Fig. 1b) and a symptomatic rat pup with NEC by traditional histologic scoring (Fig. 1c). However, closer examination of Figure 1b demonstrates an early-stage intestinal alteration, as demonstrated by expansion of the submucosal layer indicated by blue arrows. Figure 1c shows a higher degree of submucosal space expansion together with villus disruption. The thickness of the submucosal layer (see Fig. 1a–c) of the control pup was 38 ± 7 μm (Fig. 1a), and was significantly increased for the stressed pup even without histologic evidence of villus injury at 112 ± 15 μm (Fig. 1b) and in the pup with NEC at 158 ± 19 μm (Fig. 1c). The changes in wall thickness (~100–150 μm) are too small to be accurately measured using the MRI protocols with 100–200 μm in-plane resolution, as listed in Table 1. Therefore, MRI studies focused on the use of T_2 and diffusion imaging to discriminate between the control and NEC groups, including pups with mild edema in the ileum without histologic evidence of NEC.

To determine whether MRI could be used to identify this early expansion of the submucosal layer, we established methods for the consistent identification of the ileum in MR images. Figure 2 shows a photograph of a control rat pup (Fig. 2a) placed on a temperature-resistant garolite holder before insertion into the quad coil and the magnet, and MR images (Fig. 2b–d) of the same pup. MR images were acquired from rectum to chest cavity (the length of the imaged area was about 15 mm), as indicated by the ruler in Fig. 2a. The stomach, cecum, small bowel, kidneys and chest cavity are labeled in the MR images. The identification of the cecum is very important because it provides the point of reference for the identification of the ileum adjacent to the cecum. The axial images in Fig. 2 show normal ileum, with no hyperintensity associated with edema or inflammation, as expected for a mother-fed, normal rat pup.

We acquired high-resolution MR images in both coronal and axial planes to identify intestinal damage in regions adjacent to the cecum. Figure 3 compares coronal and axial T_2-weighted MR images of control (Fig. 3a, c) and stressed (Fig. 3b, d) rat pups. In NEC pups, inflamed regions of the ileum, indicated by red arrowheads, appear much brighter (Fig. 3b, d) than the corresponding regions in control pups (Fig. 3a, c). MR images of a NEC pup show hyperintense ileum associated with edema.

We next determined whether MRI could identify edema on the basis of measured ADC and T_2 values. Examples of ADC and T_2 maps are shown in Figure 4. Figure 4a, d compares T_2-weighted MR images of three sequential MRI slices from a control and NEC pup, respectively. The pixel size is 200 μm × 200 μm. In the MR images of both panels (Fig. 4a, d), the cecum is indicated by white arrows, whereas ileum regions, immediately proximal to the cecum, are indicated by green or red arrowheads for the control and NEC pup, respectively. Brighter ileal sections corresponding to the inflamed ileum are seen only in images in Figure 4d for the NEC pup (NEC score of 3), whereas, for the healthy control pup (Fig. 4a), no inflammation is detected. T_2 and ADC maps for both pups are also shown in Figure 4. In each case, we manually selected a small area of 0.5–0.6 mm^2 (with about 85–105 pixels) of the ileal section adjacent to the cecum as the ROI for the measurement of T_2 and ADC values. These regions are outlined in black in Figure 4b, c, e, f. The ROIs in NEC pups contain multiple red pixels, indicating high T_2 and ADC. The ROIs in control pups do not contain red pixels, indicating that there are no high T_2 or ADC values.

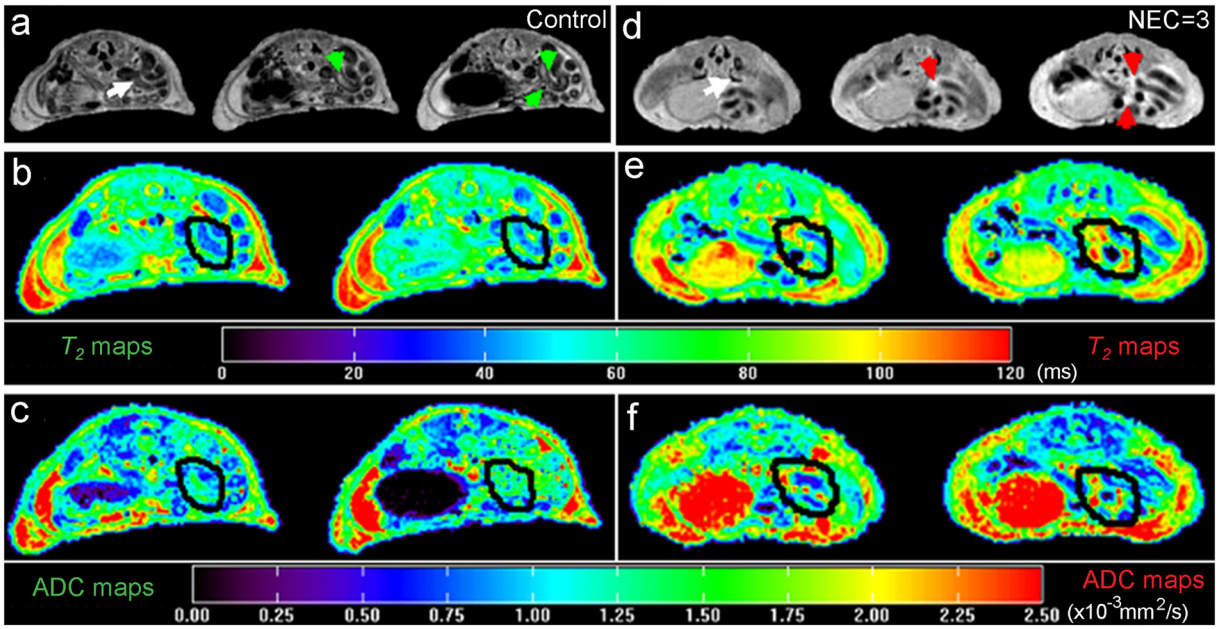

Figure 4. Comparison of MR images of the intestine, together with T_2 and apparent diffusion coefficient (ADC) maps, of a control pup and a rat pup with a necrotizing enterocolitis (NEC) score of 3. (a–c) T_2-weighted MR images and T_2 and ADC maps of a 3-day-old, mother-fed, nonstressed control rat pup. (a) T_2-weighted MR images of the three sequential MRI slices (thickness, 0.5 mm) from a control pup, in which the cecum is indicated by a white arrow and the ileum regions adjacent to the cecum are indicated by green arrowheads. (b, c) Corresponding T_2 and ADC maps, respectively, for the two right-most MRI slices, proximal to the cecum, as shown in (a). Color bars with values for T_2 and ADC maps are also illustrated. (d–f) Corresponding MR images and maps of the ileal section of a symptomatic rat pup with NEC. (d) The cecum is indicated by the white arrow, whereas its adjacent ileal regions are indicated by red arrowheads. In the NEC pups, the areas circled in black in (e) and (f) show more yellow and red, indicating that the ileal regions of a symptomatic rat pup with NEC have higher T_2 and ADC values than those of the control rat pups, with mostly blue and green in the areas circled in black in (b) and (c).

Mono-exponential decays [Equations [1] and [2]] provided excellent fits to T_2 and ADC data. The plot in Figure 5a compares T_2 and ADC values as a function of intestinal injury. T_2 and ADC values for the ileal regions of stressed, 'pre'-NEC pups [n = 5; T_2 = 79.1 ± 3.1 ms, ADC = (1.31 ± 0.07) × 10^{-3} mm^2/s], and pups with NEC scores of 1 [n = 5; T_2 = 90.3 ± 3.7 ms, ADC = (1.51 ± 0.09) × 10^{-3} mm^2/s], 2 [n = 3; T_2 = 99.9 ± 3.9 ms, ADC = (1.81 ± 0.10) × 10^{-3} mm^2/s] and 3 [n = 3; T_2 = 110.1 ± 4.2 ms, ADC = (2.11 ± 0.09) × 10^{-3} mm^2/s], were significantly higher than those for control pups [n = 15; T_2 = 64.9 ± 2.3 ms, ADC = (1.10 ± 0.06) × 10^{-3} mm^2/s). The average values of T_2 and ADC of each group were statistically significantly different from those of the other groups, e.g. 'pre'-NEC *versus* NEC score of 0, or NEC score of 1 *versus* NEC score of 2, etc., with $p < 0.01$. T_2 and ADC increased monotonically as a function of NEC score. Figure 5b demonstrates the difference between plots of signal *versus* TE in ROI with areas of 0.5 mm^2 in control pups and pups with NEC scores of 1, 2 and 3; the fits and measured T_2 values in the four ROIs are significantly different ($p < 0.01$).

In Table 2, we summarize the results of four groups: (i) healthy control, mother-fed rat pups; (ii) experimental control pups that were prematurely born, formula fed and stressed, but had no sign of NEC on histology or intestinal inflammation by MRI; (iii) pups with no abdominal distension and mild expansion of the submucosal layer, NEC score of <2; (iv) pups with abdominal distension and a higher degree of expansion of the submucosal layer, NEC score of ≥2. The first two groups are 'controls' as they showed no sign of NEC. The third and fourth groups separate rat pups who have significant disease (NEC score of ≥2) from those who do not have significant disease (NEC score of <2). As indicated in Table 2, based on the measured T_2 and ADC values of these three groups, there is a statistically significant difference between control pups, early intestinal injury pups (NEC score of <2) and pups with NEC (NEC score of ≥2) with $p < 0.03$.

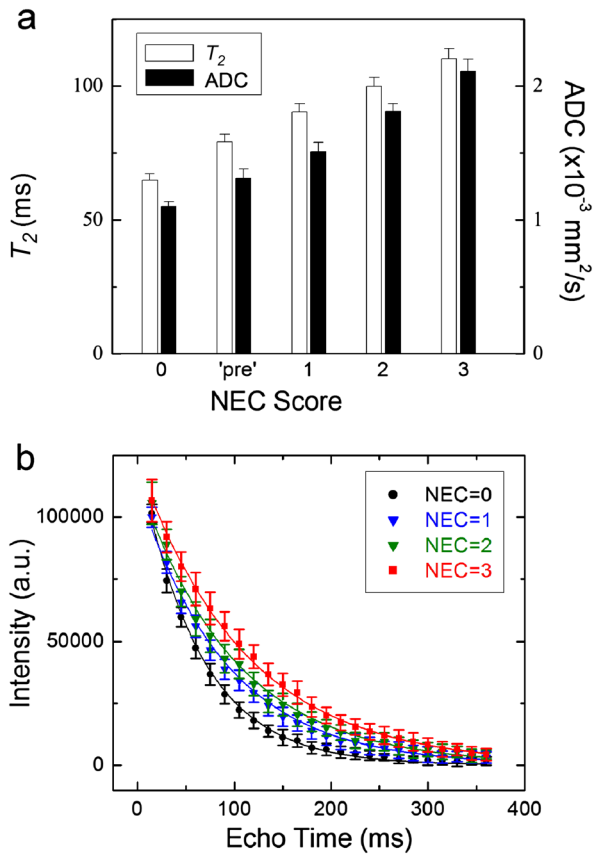

Figure 5. Comparison of MRI-determined values of T_2 and apparent diffusion coefficient (ADC) of a control pup and rat pups with necrotizing enterocolitis (NEC). (a) Plot of T_2 and ADC values as a function of NEC score. T_2 and ADC values were determined directly from the corresponding maps shown in Fig. 4, whereas NEC scores were determined from hematoxylin and eosin-stained slices. Values of T_2 and ADC for each group, indicated on the ordinate as the degree of inflammation, are statistically significant ($p < 0.01$). The numbers of control and NEC pups are given in the Materials and methods section. (b) MRI-determined T_2 plots of a control pup (NEC score of 0) and pups with NEC scores of 1, 2 and 3. The signal intensities are plotted as a function of TE. An area of 0.5 mm^2 (about 85 pixels) as a region of interest in each case was chosen to obtain intensities with TE. The steeper slope for the control pup indicates a lower T_2 value compared with the same ileum region in pups with NEC scores of 1, 2 or 3 ($p < 0.01$). All plots are labeled and color coded according to NEC score.

DISCUSSION

Neonatal NEC is a devastating intestinal inflammatory disorder of premature infants that remains poorly understood and lacks specific therapy. Current research is hampered by the inability to diagnose NEC in research models and thus to intervene prior to animal sacrifice. The study reported here addresses this deficit. These results demonstrate that, with an appropriate anesthesia protocol, high-resolution images with excellent contrast can be obtained from neonatal rat pups using the most widely employed rodent model of NEC. Values of T_2 and ADC in the ileum correlated well with NEC values determined from histology. In addition, T_2 and ADC values were higher in rat pups with 'pre'-NEC than in control pups. The values of T_2 and ADC for the ileum were significantly higher in NEC pups than in stressed pups with no NEC and in healthy control pups. This suggests that MRI can provide an early, noninvasive diagnosis of NEC, and may also be useful for monitoring the response to therapy in experimental models. The high-resolution anatomic and functional images shown here suggest that MRI studies of the neona-

Table 2. MRI-determined values of the spin–spin relaxation time (T_2) and the apparent diffusion coefficient (ADC) of 3-day-old rat pups as a function of necrotizing enterocolitis (NEC)[a]

Group	T_2 (ms)	ADC (×10^{-3} mm^2/s)
Control (n = 15)	64.9 ± 2.3	1.10 ± 0.06
NEC score of 0 (n = 20)[b]	66.3 ± 3.1	1.08 ± 0.07
NEC score of <2 (n = 10)	85.2 ± 6.8	1.43 ± 0.16
NEC score of ≥2 (n = 6)	106.3 ± 6.1	1.98 ± 0.15

[a]MRI-determined values of T_2 and ADC are presented as means ± standard deviation. Measured values of T_2 and ADC were compared between the control groups and the diseased groups (NEC score of <2 and NEC score of ≥2) by two-way analysis of variance, and were found to be statistically significantly different ($p < 0.03$).

[b]Experimental control pups that were prematurely born, formula fed and stressed, but had no sign of NEC on histology or intestinal inflammation by MRI.

tal rat pup model noninvasively identify early intestinal injury, and could guide the development of new treatments for NEC.

The development of NEC is associated with extensive inflammation (7,11). Inflamed regions of ileum in rat pups with NEC are expected to be edematous and thus to have increased water content, which would increase the T_2 value relative to normal ileum (12), consistent with the results reported here. The measured ADC reflects both the cell density and the water content (24). Inflammatory cell infiltrate of the affected region of rat pups with NEC is expected to have a relatively low cell density; for example, the hematoxylin and eosin-stained tissue in Figure 1c shows decreased density of cells and changes in crypt morphology, seen as disruption of the villus. This is consistent with the higher ADC measured by DWI.

To our knowledge, this is the first report of MRI studies of NEC in any animal model. Indeed, no abdominal MRI studies have been reported for a 2–4-day-old neonatal animal model. It is likely that further optimization of data acquisition and analysis will improve the strength of the correlation between MRI parameters and histology, and perhaps facilitate the analysis of data on a pixel-by-pixel basis. Furthermore, studies of a larger number of animals at each stage of NEC are needed to define a scale of MRI parameters or combinations of MRI parameters that can be used to reliably assess the disease state noninvasively. Despite the need for further development and testing of this approach, the results presented here are promising and suggest that MRI can reliably and accurately assess NEC and response of NEC to therapy.

CONCLUSIONS

This article provides a method for noninvasive imaging studies of the early initiation of intestinal injury and efficacy of treatment options for this disease. As the neonatal rat model studied here is widely used, a noninvasive means of diagnosing early intestinal injury in animal models of NEC will have significant impact on research into this disease. A noninvasive tool for the diagnosis of NEC at an early stage could potentially be translated to clinical utility. The MRI protocol as listed in Table 1 is clearly too lengthy to be used clinically. Once the most promising parameters and analysis methods have been identified, the protocol for the evaluation of NEC could be significantly shortened to allow routine clinical scans of patients. It is likely that clinical scans will be faster because of parallel imaging and partial Fourier sampling methods. In addition, it has been shown recently that with three b values of 0, 1000 and 2000 s/mm^2, multi-slice diffusion-weighted images can be acquired within about 3 min and 20 s on a clinical magnet of 3 T (25). Therefore, we estimate that for one spoiled GE (2 min), one FSE (5 min), one MSME (4 min) and one DWI (4 min), we need about 15 min for data acquisition. Earlier diagnosis with MRI could lead to earlier intervention and thus decreased morbidity in patients.

Acknowledgements

This work was supported by grants from the National Institutes of Health (RO1-HD059123 to E.C.C.), Digestive Disease Research Core Center of the University of Chicago (P30DK42086), a Clinical and Translational Science Award to the University of Chicago Medical Center (UL1-RR024999) and the Lynn S. Florsheim MRIS facility.

REFERENCES

1. Fanaroff AA, Stoll BJ, Wright LL, Carlo WA, Ehrenkranz RA, Stark AR, Bauer CR, Donovan EF, Korones SB, Laptook AR, Lemons JA, Oh W, Papile LA, Shankaran S, Stevenson DK, Tyson JE, Poole WK. Trends in neonatal morbidity and mortality for very low birthweight infants. Am. J. Obstet. Gynecol. 2007; 196(2): 147e141–147e148.
2. Hintz SR, Kendrick DE, Stoll BJ, Vohr BR, Fanaroff AA, Donovan EF, Poole WK, Blakely ML, Wright L, Higgins R. Neurodevelopmental and growth outcomes of extremely low birth weight infants after necrotizing enterocolitis. Pediatrics 2005; 115(3): 696–703.
3. Lemons JA, Bauer CR, Oh W, Korones SB, Papile LA, Stoll BJ, Verter J, Temprosa M, Wright LL, Ehrenkranz RA, Fanaroff AA, Stark A, Carlo W, Tyson JE, Donovan EF, Shankaran S, Stevenson DK. Very low birth weight outcomes of the National Institute of Child health and human development neonatal research network, January 1995 through December 1996. NICHD Neonatal Research Network. Pediatrics 2001; 107(1): E1.
4. Martin CR, Walker WA. Probiotics: role in pathophysiology and prevention in necrotizing enterocolitis. Semin. Perinatol. 2008; 32(2): 127–137.
5. Caplan MS, Hedlund E, Adler L, Hsueh W. Role of asphyxia and feeding in a neonatal rat model of necrotizing enterocolitis. Pediatr. Pathol. 1994; 14(6): 1017–1028.
6. Caplan MS, Miller-Catchpole R, Kaup S, Russell T, Lickerman M, Amer M, Xiao Y, Thomson R Jr. Bifidobacterial supplementation reduces the incidence of necrotizing enterocolitis in a neonatal rat model. Gastroenterology, 1999; 117(3): 577–583.
7. Caplan MS, Russell T, Xiao Y, Amer M, Kaup S, Jilling T. Effect of polyunsaturated fatty acid (PUFA) supplementation on intestinal inflammation and necrotizing enterocolitis (NEC) in a neonatal rat model. Pediatr. Res. 2001; 49(5): 647–652.
8. Clark JA, Doelle SM, Halpern MD, Saunders TA, Holubec H, Dvorak K, Boitano SA, Dvorak B. Intestinal barrier failure during experimental necrotizing enterocolitis: protective effect of EGF treatment. Am. J. Physiol. Gastrointest. Liver Physiol. 2006; 291(5): G938–G949.
9. Jilling T, Simon D, Lu J, Meng FJ, Li D, Schy R, Thomson RB, Soliman A, Arditi M, Caplan MS. The roles of bacteria and TLR4 in rat and murine models of necrotizing enterocolitis. J. Immunol. 2006; 177(5): 3273–3282.
10. Nadler EP, Dickinson E, Knisely A, Zhang XR, Boyle P, Beer-Stolz D, Watkins SC, Ford HR. Expression of inducible nitric oxide synthase and interleukin-12 in experimental necrotizing enterocolitis. J. Surg. Res. 2000; 92(1): 71–77.
11. Shiou SR, Yu Y, Chen S, Ciancio MJ, Petrof EO, Sun J, Claud EC. Erythropoietin protects intestinal epithelial barrier function and lowers the incidence of experimental neonatal necrotizing enterocolitis. J. Biol. Chem. 2011; 286(14): 12 123–12 132.
12. Mustafi D, Fan X, Dougherty U, Bissonnette M, Karczmar GS, Oto A, Hart J, Markiewicz E, Zamora M. High-resolution magnetic resonance colonography and dynamic contrast-enhanced magnetic resonance imaging in a murine model of colitis. Magn. Reson. Med. 2010; 63(4): 922–929.
13. Mansfield P, Morris PG, Ordidge RJ, Pykett IL, Bangert V, Coupland RE. Human whole body imaging and detection of breast tumours by n.m.r. Philos. Trans. R. Soc. London, B: Biol. Sci. 1980; 289(1037): 503–510.
14. Rzedzian R, Chapman B, Mansfield P, Coupland RE, Doyle M, Chrispin A, Guilfoyle D, Small P. Real-time nuclear magnetic resonance clinical imaging in paediatrics. Lancet 1983; 2(8362): 1281–1282.
15. Esserman L, Wolverton D, Hylton N. Magnetic resonance imaging for primary breast cancer management: current role and new applications. Endocr. Relat. Cancer, 2002; 9(2): 141–153.
16. Genovese E, Cani A, Rizzo S, Angeretti MG, Leonardi A, Fugazzola C. Comparison between MRI with spin-echo echo-planar diffusion-weighted sequence (DWI) and histology in the diagnosis of soft-tissue tumours. Radiol. Med. 2011; 116(4): 644–656.
17. Johnson DA, Helft PR, Rex DK. CT and radiation-related cancer risk-time for a paradigm shift? Nat. Rev. Gastroenterol. Hepatol. 2009; 6(12): 738–740.
18. Nickoloff EL, Alderson PO. Radiation exposures to patients from CT: reality, public perception, and policy. Am. J. Roentgenol. 2001; 177 (2): 285–287.
19. Sadetzki S. Excess lifetime cancer mortality risk attributed to radiation exposure from pediatric computed tomography scan. Isr. Med. Assoc. J. 2007; 9(8): 607–609.

20. Maalouf EF, Fagbemi A, Duggan PJ, Jayanthi S, Counsell SJ, Lewis HJ, Fletcher AM, Lakhoo K, Edwards AD. Magnetic resonance imaging of intestinal necrosis in preterm infants. Pediatrics 2000; 105(3 Pt 1): 510–514.
21. Buisson A, Joubert A, Montoriol PF, Da Ines D, Hordonneau C, Pereira B, Garcier JM, Bommelaer G, Petitcolin V. Diffusion-weighted magnetic resonance imaging for detecting and assessing ileal inflammation in Crohn's disease. Aliment. Pharmacol. Ther. 2013; 37(5): 537–545.
22. Israel EJ. Neonatal necrotizing enterocolitis, a disease of the immature intestinal mucosal barrier. Acta Paediatr. Suppl. 1994; 396: 27–32.
23. Haney CR, Fan X, Markiewicz E, Mustafi D, Karczmar GS, Stadler WM. Monitoring anti-angiogenic therapy in colorectal cancer murine model using dynamic contrast-enhanced MRI: comparing pixel-by-pixel with region of interest analysis. Technol. Cancer Res. Treat. 2013; 12(1): 71–78.
24. Ginat DT, Mangla R, Yeaney G, Johnson M, Ekholm S. Diffusion-weighted imaging for differentiating benign from malignant skull lesions and correlation with cell density. Am. J. Roentgenol. 2012; 198(6): W597–W601.
25. Ueno Y, Kitajima K, Sugimura K, Kawakami F, Miyake H, Obara M, Takahashi S. Ultra-high b-value diffusion-weighted MRI for the detection of prostate cancer with 3-T MRI. J. Magn. Reson. Imaging 2013; 38(1): 154–160.